RAPID COMMUNICATION

Stability of the topological quantum critical point between multi-Weyl semimetal and band insulator

Zhao-Kun Yang(杨兆昆)[1], Jing-Rong Wang(王景荣)[2], and Guo-Zhu Liu(刘国柱)[1,†]

[1] *Department of Modern Physics, University of Science and Technology of China, Hefei* 230026, *China*
[2] *High Magnetic Field Laboratory of Anhui Province, Chinese Academy of Sciences, Hefei* 230031, *China*

(Received 21 October 2022; revised manuscript received 10 February 2023; accepted manuscript online 10 February 2023)

One could tune a topological double-Weyl semimetal or a topological triple-Weyl semimetal to become a topologically trivial insulator by opening a band gap. This kind of quantum phase transition is characterized by the change of certain topological invariant. A new gapless semimetallic state emerges at each topological quantum critical point. Here we perform a renormalization group analysis to investigate the stability of such critical points against perturbations induced by random scalar potential and random vector potential. We find that the quantum critical point between double-Weyl semimetal and band insulator is unstable and can be easily turned into a compressible diffusive metal by any type of weak disorder. The quantum critical point between triple-Weyl semimetal and band insulator flows to a stable strong-coupling fixed point if the system contains a random vector potential merely along the z-axis, but becomes a compressible diffusive metal when other types of disorders exist.

Keywords: topological quantum critical points, Weyl semimetal, disorder, renormalization group

PACS: 64.60.Ht, 64.60.ae, 64.70.Tg **DOI:** 10.1088/1674-1056/acbaf2

1. Introduction

Semimetal (SM) materials have attracted tremendous research activities in the past two decades,[1–14] partly due to the potential industrial applications and partly due to the unique properties. There are two different ways to realize SM materials. First, some SM materials are intrinsic and their stability is protected by symmetries of the system.[2–8] Examples include three-dimensional (3D) Dirac SMs (DSMs), such as Cd_3As_2, Na_3Bi, Weyl SMs (WSMs), such as TaAs, TaP, NbAs, NbP, and nodal line SMs (NLSMs), such as ZrSiS and $PbTaSe_2$. Alternatively, SM state can be realized by tuning a system to undergo a quantum phase transition between two quantum states of matter that are characterized by two different topological invariants.[15–25] Usually, a specific SM state emerges at the topological quantum critical point (TQCP) of this transition. For example, the TQCP between 3D topological insulator and trivial band insulator (BI) is described by a 3D DSM state. This type of 3D DSM has been observed in $TiBiSe_{2-x}S_x$[26,27] and $Bi_{2-x}In_xSe_3$[28,29] by fine tuning the doping level. Another example is the TQCP between two-dimensional (2D) DSM and BI, at which there exists a 2D semi-DSM phase.[16–20] The low-energy fermions excited in such a 2D semi-DSM phase exhibit a linear dispersion along one direction and a quadratic dispersion along the other.

Besides the usual WSMs, multi-WSMs, including double-WSM and triple-WSM, have also attracted extensive interests.[30–39] For usual, double-, and triple-WSMs, the monopole charges of a pair of Weyl points are equal to ±1, ±2, and ±3, respectively. In double-WSMs (triple-WSMs), the fermion dispersion is always linear along one direction, but quadratic (cubic) along the rest two directions. Recent investigations have revealed two candidate materials for double-WSM, including $HgCr_2Se_4$[31] and $SrSi_2$.[40] Cubic-Dirac SM (cubic-DSM), in which the fermion dispersion is cubic along two directions and linear along the third one, is suggested to emerge in $Rb(MoTe)_3$ and $Tl(MoTe)_3$, which belong to the $A(MoX)_3$ family.[41] Multi-Weyl fermions may also be realized by manipulating photonic crystals.[42,43]

WSM materials provide a flexible platform to create new types of gapless SM phases.[3,21–25] One can open a band gap to a usual WSM by tuning some external parameters, which turns usual WSM into an ordinary BI. The usual WSM and BI are topologically distinct, hence the transition between these two phases should be identified as a topological phase transition. At the TQCP of this transition, the system exhibits a gapless SM state in which the fermionic excitations disperse linearly along two directions and quadratically along the third one.[21,22] One can manipulate double- and triple-WSM materials analogously and drive them to become BIs. Such a manipulation then leads to a double-TQCP and a triple-TQCP, respectively. At the former TQCP, the gapless low-energy fermions have a quadratic dispersion along all three directions.[24,25] At the latter TQCP, the gapless low-energy fermions have a dispersion that is cubic along two directions and quadratic along the third one.[23]

In practice, it would be difficult to realize double- and

†Corresponding author. E-mail: gzliu@ustc.edu.cn

© 2023 Chinese Physical Society and IOP Publishing Ltd

triple-TQCPs if they are unstable against weak perturbations. In particular, we need to examine the stability of these TQCPs against disorder scattering, since disordered potentials are always present in realistic materials. According to how fermions are coupled to randomly distributed potentials, disorders in SM materials are usually classified into three types, namely, random scalar potential (RSP), random vector potential (RVP), and random mass (RM). Extensive previous studies[15,34,44–64] revealed that the physical effects of disorders depend sensitively on the fermion dispersion, the spatial dimensionality, and the characters of the disordered potential. For instance, renormalization group (RG) studies[44–47] found that RSP, RVP, and RM in a 2D DSM are relevant, marginal, and marginally irrelevant, respectively. In the clean limit, the noninteracting Dirac fermions in a 2D DSM can propagate freely, with an infinitely long lifetime, and have a vanishing density of states (DOS) at the Fermi level. These behaviors are significantly changed once disorders are considered. It was found[15,48–52] that an arbitrary weak RSP suffices to generate a finite disorder scatting rate for Dirac fermions. As a consequence, the Dirac fermions acquire a shortened lifetime and a finite DOS at the Fermi level. Apparently, RSP drives the 2D DSM to undergo a transition into a distinct phase, which is usually called a compressible diffusive metal (CDM) in the literature. The finite disorder scattering rate can thus be regarded as the signature for the emergence of CDM. In contrast, RVP and RM do not drive any phase transition, but result in power-law or logarithmic-like corrections to the energy- or temperature-dependence of various observable quantities. For a 3D DSM or a WSM, RSP is shown[34,52–54] to be irrelevant in the weak disorder region. If the disorder strength exceeds a threshold, RSP becomes relevant and drives the SM phase into a CDM Phase. It appears that one single component of RVP is always irrelevant in ordinal WSM. However, the coexistence of two components of RVP is capable of triggering a SM-to-CDM transition in the strong disorder region.[56]

The disorder effects on double- and triple-WSMs have been investigated extensively. Similar to 2D DSM, the double-WSM undergoes a transition into a CDM phase if there is an arbitrary weak random potential.[34,37] However, a triple-WSM that contains certain component of RVP could realize a stable quantum critical state in which observable quantities receive power-law corrections owing to the fermion-disorder coupling.[37] Recently, Luo *et al.*[61,62] and Roy *et al.*[63] analyzed the influence of disorders at the TQCP between usual WSM and BI. According to their RG calculations, while weak disorders are irrelevant, sufficiently strong disorders become relevant and are capable of triggering a transition into CDM phase. To the best of our knowledge, the effects of various disorders at the TQCPs between multi-WSMs and BI have not been studied previously.

In this paper, we consider the stability of double- and triple-TQCPs against disorders by using the RG approach. There are four types of disorders at such TQCPs, including RSP and the three spatial components of RVP. After deriving the self-consistent flow equations of all the model parameters, we show that double- and triple-TQCPs behave differently in response to disorders. For double-TQCP, the system is unstable against weak disorders and can be turned into CDM phase by any type of random potential. In particular, coupling the fermions to RSP alone or to any component of RVP suffices to dynamically generate all the other disorders. The triple-TQCP is also unstable towards a CDM transition if there is only RSP, x-RVP, or y-RVP. Any of the three disorders of RSP, x-RVP, and y-RVP is capable of generating the rest. However, the z-RVP has a quite different impact on triple-TQCP. Due to the peculiar fermion dispersion at triple-TQCP, z-RVP cannot generate other disorders. Our RG analysis demonstrates that triple-TQCP exhibits a stable quantum critical state if the system contains merely z-RVP. In the lowest energy limit, this quantum critical state is found to be at a strong-coupling fixed point.

The rest of paper will be arranged as follows. In Section 2 we define the effective models for double- and triple-TQCPs. In Section 3 we obtain the coupled RG equations for all the model parameters and analyze the physical effects of various disorders in order to determine whether TQCPs are stable against disorder-induced perturbations. In Section 4 we summarize the results of this paper and discuss some further research projects.

2. Models for topological quantum critical points

The double-TQCP can be described by the Hamiltonian[24,25]

$$H_{\mathrm{f}}^{\mathrm{d}} = \int \mathrm{d}^3\boldsymbol{x}\,\psi^{\dagger}(\boldsymbol{x})\big[-A_{\perp}\left(\partial_x^2-\partial_y^2\right)\sigma_1 - A_{\perp}\partial_x\partial_y\sigma_2 - A_z\partial_z^2\sigma_3\big]\psi(\boldsymbol{x}), \tag{1}$$

where ψ is a two-component spinor field and $\sigma_{1,2,3}$ are the Pauli matrices. The energy dispersion of fermions is

$$E_{\pm}^{\mathrm{d}}(\boldsymbol{k}) = \pm\sqrt{A_{\perp}^2k_{\perp}^4+A_z^2k_z^4}, \tag{2}$$

where $k_{\perp}$ is defined as $k_{\perp}\equiv\sqrt{k_x^2+k_y^2}$, the model parameters $A_{\perp}$ and A_z are material dependent. The fermion dispersion is schematically plotted in Fig. 1.

The free fermion propagator has the form

$$G_{\mathrm{d}0}(\mathrm{i}\omega,\boldsymbol{k}) = \frac{1}{\mathrm{i}\omega - A_{\perp}\left(k_x^2-k_y^2\right)\sigma_1 - 2A_{\perp}k_xk_y\sigma_2 - A_zk_z^2\sigma_3}. \tag{3}$$

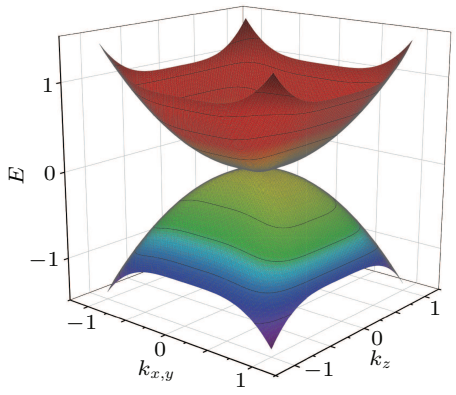


Fig. 1. Dispersion of the low-energy fermions excited at double-TQCP.

For triple-TQCP, the Hamiltonian of fermions[23] is given by

$$H_{\mathrm{f}}^{\mathrm{t}} = \int \mathrm{d}^3\boldsymbol{x}\psi^{\dagger}(\boldsymbol{x})\left[\mathrm{i}B\left(\partial_x^3 - 3\partial_x\partial_y^2\right)\sigma_1 + \mathrm{i}B\left(\partial_y^3 - 3\partial_y\partial_x^2\right)\sigma_2 - A\partial_z^2\sigma_3\right]\psi(\boldsymbol{x}). \tag{4}$$

The corresponding fermion dispersion is

$$E_{\pm}^{\mathrm{t}}(\boldsymbol{k}) = \pm\sqrt{B_{\perp}^2 k_{\perp}^6 + A^2 k_z^4}, \tag{5}$$

which is visualized in Fig. 2. Here we introduce two other model parameters B and A.

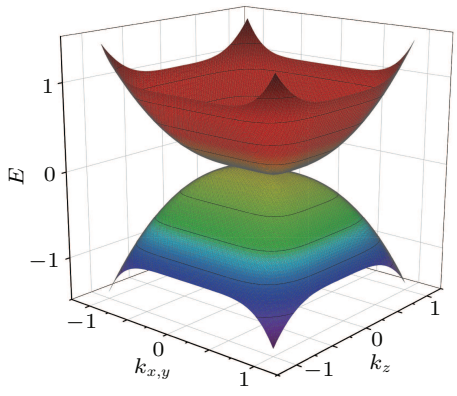


Fig. 2. Dispersion of the low-energy fermions excited at triple-TQCP.

The fermion propagator is

$$G_{\mathrm{t}0}(\mathrm{i}\omega,\boldsymbol{k}) = \frac{1}{\mathrm{i}\omega - B\left(k_x^3 - 3k_xk_y^2\right)\sigma_1 - B\left(k_y^3 - 3k_yk_x^2\right)\sigma_2 - Ak_z^2\sigma_3}. \tag{6}$$

To describe the disorder scattering of fermions, it is convenient to introduce a number of random potentials, denoted by $V(\boldsymbol{x})$, and couple these potentials to fermions as follows:[65,66]

$$H_{\mathrm{dis}} = \sum_{j=0}^{3}\int \mathrm{d}^3\boldsymbol{x}V_j(\boldsymbol{x})\psi^{\dagger}(\boldsymbol{x})\Gamma_j\psi(\boldsymbol{x}). \tag{7}$$

The potentials $V_j(\boldsymbol{x})$ are static in time but randomly distributed in 3D space. Such potentials are usually supposed to be Gaussian white noise and satisfy the following relations:

$$\left\langle V_j(\boldsymbol{x})\right\rangle = 0, \quad \left\langle V_j(\boldsymbol{x})V_j(\boldsymbol{x}')\right\rangle = \Delta_j\delta^3\left(\boldsymbol{x}-\boldsymbol{x}'\right). \tag{8}$$

The random potentials need to be averaged. With the help of the widely used replica trick,[47] we convert the fermion-disorder coupling into a new term

$$H_4 = \sum_{j=0}^{3}\frac{\Delta_j}{2}\int \mathrm{d}\tau\mathrm{d}\tau'\mathrm{d}^3\boldsymbol{x}\left(\psi_a^{\dagger}\Gamma_j\psi_a\right)_{\tau}\left(\psi_b^{\dagger}\Gamma_j\psi_b\right)_{\tau'}, \tag{9}$$

where $a,b = 1,2,\ldots,n$ are replica indexes. The limit $n\to 0$ should be taken at the end of calculations. At the TQCPs, there might exist various forms of disorders. Each matrix Γ_j is used to define a special type of disorder. RSP is defined via the unit matrix $\Gamma_0 = \mathbb{1}$. The three components of RVP are defined by three matrices $\Gamma_{1,2,3} = \sigma_{1,2,3}$. Throughout this paper, we shall use x-RVP, y-RVP, and z-RVP to represent the x, y, and z components of RVP, respectively.

For each type of random field V_j, its effective strength is measured by a specific strength parameter Δ_j. For a given material, the value of Δ_j is regarded as a constant in the non-interacting limit. The interaction between free fermions and random potentials renormalizes all the model parameters. Under proper conditions, this interaction could trigger an instability of the system towards a new phase. In the next section, we carry out a RG analysis to obtain the flow equations of all the model parameters and investigate the stability of double- and triple-TQCPs.

3. Renormalization group analysis

In order to perform RG analysis,[67] one needs to first define the action of a TQCP at a high energy scale Λ, which serves as an ultraviolet (UV) cutoff. The cutoff Λ can be quantitatively determined by the lattice spacing. But the precise value of Λ is unimportant and does not affect the final RG results. Now let us introduce a tuning parameter b and use this parameter to define a momentum shell $b\Lambda < \sqrt{A_{\perp}^2k_{\perp}^4 + A_z^2k_z^4} < \Lambda$ for double-TQCP and a momentum shell $b\Lambda < \sqrt{B^2k_{\perp}^6 + A^2k_z^4} < \Lambda$ for triple-TQCP. Then we integrate over all the modes inside the momentum shell by using the functional integral formalism.[67] The action obtained after such calculations is defined in the reduced range of $[0, b\Lambda]$. Next, we re-scale all the field operators and all the model parameters, and obtain a new action defined in the range of $[0,\Lambda]$. Comparing this new action to the original action, we would be able to determine how the model parameters flow as the energy scale is changed.[67] We are especially interested in the low-energy behavior of the model parameters. For this purpose, we follow Ref. [67] and introduce a freely varying parameter ℓ to express b as $b = \mathrm{e}^{-\ell}$. At the UV cutoff Λ, $\ell = 0$.

In the lowest-energy limit, $\ell \to +\infty$. The RG flow of a model parameter can be well described by the ℓ-dependence of this parameter.[67] The detailed RG calculations are presented in Appendix A. Below we only provide the final RG equations.

For double-TQCP, we obtain the following flow equations for the model parameters:

$$\frac{\mathrm{d}A_\perp}{\mathrm{d}\ell} = -\frac{9}{2}(\Delta_0+\Delta_1+\Delta_2+\Delta_3)A_\perp, \tag{10}$$

$$\frac{\mathrm{d}A_z}{\mathrm{d}\ell} = -\frac{9}{2}(\Delta_0+\Delta_1+\Delta_2+\Delta_3)A_z, \tag{11}$$

$$\frac{\mathrm{d}\Delta_0}{\mathrm{d}\ell} = \frac{1}{2}\Delta_0+\frac{39}{4}\Delta_0^2+\frac{103}{4}\Delta_0(\Delta_1+\Delta_2+\Delta_3), \tag{12}$$

$$\frac{\mathrm{d}\Delta_1}{\mathrm{d}\ell} = \frac{1}{2}\Delta_1-\frac{25}{4}\Delta_0\Delta_1+8\Delta_0^2+\frac{7}{4}\Delta_1^2 +8\Delta_2^2+8\Delta_3^2+\frac{71}{4}\Delta_1(\Delta_2+\Delta_3), \tag{13}$$

$$\frac{\mathrm{d}\Delta_2}{\mathrm{d}\ell} = \frac{1}{2}\Delta_2-\frac{25}{4}\Delta_0\Delta_2+8\Delta_0^2+8\Delta_1^2 +\frac{7}{4}\Delta_2^2+8\Delta_3^2+\frac{71}{4}\Delta_2(\Delta_1+\Delta_3), \tag{14}$$

$$\frac{\mathrm{d}\Delta_3}{\mathrm{d}\ell} = \frac{1}{2}\Delta_3-\frac{25}{4}\Delta_0\Delta_3+8\Delta_0^2+8\Delta_1^2 +8\Delta_2^2+\frac{7}{4}\Delta_1^2+\frac{71}{4}\Delta_3(\Delta_1+\Delta_2). \tag{15}$$

Here, we have re-scaled four parameters Δ_j with $j=0,1,2,3$ as follows:

$$\frac{\Gamma(1/2)\Gamma(1/4)\Delta_j}{72\Gamma(3/4)\pi^2 A_\perp\sqrt{A_z\Lambda}} \to \Delta_j. \tag{16}$$

These re-scaled parameters Δ_j now become dimensionless and can be used to measure the effective strength of the disordered potentials. From this expression, one can see that increasing $A_\perp$ and/or A_z tends to reduce the values of the re-scaled Δ_j.

For triple-QCP, the flow equations for model parameters are given by

$$\frac{\mathrm{d}B}{\mathrm{d}\ell} = -6(\Delta_0+\Delta_1+\Delta_2+\Delta_3)B, \tag{17}$$

$$\frac{\mathrm{d}A}{\mathrm{d}\ell} = -6(\Delta_0+\Delta_1+\Delta_2+\Delta_3)A, \tag{18}$$

$$\frac{\mathrm{d}\Delta_0}{\mathrm{d}\ell} = \frac{5}{6}\Delta_0+\Delta_0(\Delta_0+\Delta_1+\Delta_2) +\frac{79}{7}\Delta_0\Delta_3+\frac{144}{21}(\Delta_2\Delta_3+\Delta_1\Delta_3), \tag{19}$$

$$\frac{\mathrm{d}\Delta_1}{\mathrm{d}\ell} = \frac{5}{6}\Delta_1-\frac{53}{7}\Delta_1(\Delta_0+\Delta_1)-\frac{17}{7}\Delta_1\Delta_2 +\frac{55}{7}\Delta_1\Delta_3+\frac{144}{21}\Delta_0\Delta_3, \tag{20}$$

$$\frac{\mathrm{d}\Delta_2}{\mathrm{d}\ell} = \frac{5}{6}\Delta_2-\frac{53}{7}\Delta_2(\Delta_0+\Delta_2)-\frac{17}{7}\Delta_2\Delta_1 +\frac{55}{7}\Delta_2\Delta_3+\frac{144}{21}\Delta_0\Delta_3, \tag{21}$$

$$\frac{\mathrm{d}\Delta_3}{\mathrm{d}\ell} = \frac{5}{6}\Delta_3-\frac{41}{7}\Delta_3\Delta_0-\frac{29}{7}\Delta_3(\Delta_1+\Delta_2) -\frac{5}{7}\Delta_3^2+\frac{36}{7}(\Delta_0^2+\Delta_1^2+\Delta_2^2). \tag{22}$$

Similar to the case of DQCP, we have re-scaled the parameters Δ_j as follows:

$$\frac{\Gamma(1/3)\Gamma(1/4)\Delta_j}{72\pi^2\Gamma(7/12)A^{1/2}B^{2/3}\Lambda^{5/6}} \to \Delta_j. \tag{23}$$

After performing such re-scaling transformations, Δ_j become dimensionless and serve as effective disorder strength parameters. Increasing A and/or B drives Δ_j to decrease.

3.1. Double-TQCP

We first consider double-TQCP. Suppose that the system contains only RSP at some high energy scale, at which the disorder strength parameter Δ_0 takes a small constant value. Once the coupling between RSP and fermions is taken into account, Δ_0 is renormalized and becomes a function of the varying parameter ℓ. To obtain the concrete ℓ-dependence of Δ_0, we solve the coupled RG equations given by Eqs. (10)–(15) in a self-consistent manner and present the results in Fig. 3(a). We observe that Δ_0 initially takes certain small bare value at $\ell=0$ and increases rapidly with growing ℓ as the consequence of the interaction-induced renormalization. The Δ_0 eventually flows to infinity as ℓ grows to reach a finite value ℓ_c. These results indicate that RSP is a relevant perturbation at low energies and can substantially affect the low-energy behavior of the fermions excited at double-TQCP. The runaway behavior of Δ_0 could be interpreted as a signature of the occurrence of a transition from double-TQCP into a CDM phase, which is characterized by the generation of a finite disorder scattering rate.

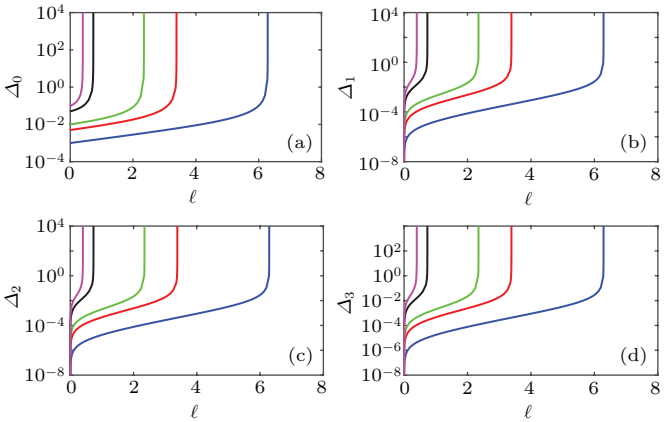


Fig. 3. Flows of disorder strength parameters at double-TQCP with pure RSP. Blue, red, green, black, magenta lines correspond to $\Delta_{0,0} = 0.001, 0.005, 0.01, 0.05, 0.1$, respectively.

The RG flows of Δ_1, Δ_2, and Δ_3 are shown in Figs. 3(b)–3(c), respectively. As we just mentioned, there is only RSP at some specific high energy scale, implying that $\Delta_1=\Delta_2=\Delta_3=0$ at $\ell=0$. As ℓ increases from zero, the coupling between fermions and RSP drives Δ_1, Δ_2, and Δ_3 to acquire nonzero values. It appears that RSP is capable of generating RVP in the

low-energy region, even though RVP does not exist at high energies. When $\ell \to \ell_c$, Δ_1, Δ_2, and Δ_3 all flow to infinity. Therefore, the dynamically generated RVP should also be identified as a relevant perturbation at low energies. The RSP and the generated RVP cooperate to turn the double-TQCP into a stable CDM phase.

Given that RSP can induce RVP, one might want to examine whether RVP could generate RSP. To address this issue, we assume that there is only one component of RVP, say x-RVP, at some high energy scale. We solve the RG equations and show the ℓ-dependence of the parameters Δ_0, Δ_1, Δ_2, and Δ_3 in Fig. 4. One can see that Δ_0 is always vanishing as ℓ grows from zero. In contrast, Δ_1 starts from a small finite value and flows at a high speed to infinity as ℓ increases. Δ_2 and Δ_3 both vanish at $\ell = 0$, but acquire nonzero values at finite ℓ. As ℓ becomes sufficiently large, Δ_1, Δ_2, and Δ_3 exhibit runaway behavior simultaneously. We obtain the same results if x-RVP is replaced with y-RVP or z-RVP. We thus draw two conclusions. First, any single component of RVP can generate other components of RVP, but can never generate RSP. Second, any single component RVP alone suffices to turn the double-TQCP to undergo a CDM transition.

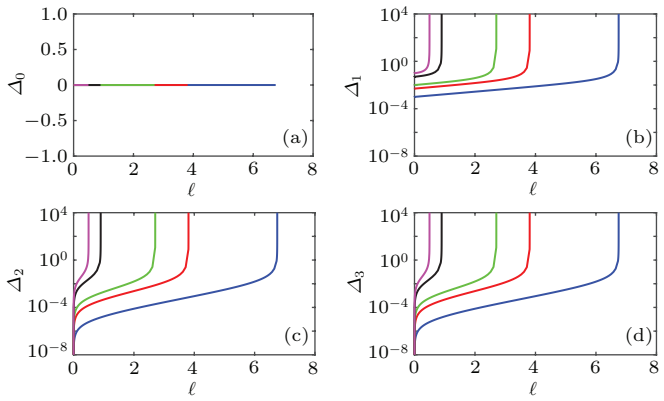


Fig. 4. Flows of disorder strength parameters at double-TQCP with pure x-RVP. Blue, red, green, black, magenta line represent $\Delta_{1,0} = 0.001, 0.005, 0.01, 0.05, 0.1$, respectively.

What is the low-energy behavior of the double-TQCP if there are two or three components of RVP at some high energy scale? We have studied these two possibilities and find that in both cases Δ_0, Δ_1, Δ_2, and Δ_3 flow to infinity. Therefore, while RSP cannot be generated by one single component of RVP, it can be generated by two or three components of RVP.

All of the above results lead us to the conclusion that the double-TQCP is unstable against disorder and can be easily turned into a CDM phase by any type of disorder.

3.2. Triple-TQCP

For triple-TQCP, we solve the RG equations of model parameters given by Eqs. (17)–(22). As in the case of double-TQCP, we are particularly interested in the stability of the triple-TQCP against disorder scattering.

Now consider the case in which only RSP exists at a chosen high energy scale with $\ell = 0$. All the model parameters begin to flow as ℓ grows from zero. The RG flows of Δ_0, Δ_1, Δ_2, and Δ_3 are depicted in Figs. 5(a)–5(d). The RSP parameter Δ_0 tends to diverge when ℓ approaches to a finite value ℓ_c. The three RVP parameters Δ_1, Δ_2, and Δ_3 develop nonzero values once ℓ becomes finite and they all diverge in the limit $\ell \to \ell_c$.

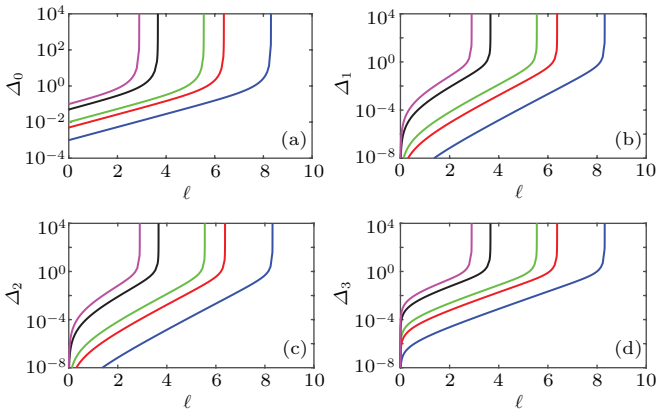


Fig. 5. Flows of disorder strength parameters at triple-TQCP with pure RSP. Blue, red, green, black, magenta lines represent $\Delta_{0,0} = 0.001, 0.005, 0.01, 0.05, 0.1$, respectively.

Next we assume that the system has only x-RVP at high energies and examine what would happen as the energy scale is lowered. According to the numerical results illustrated in Fig. 6, Δ_1 flows to infinity starting from some finite bare value and the other three parameters Δ_0, Δ_2, Δ_3 flow from zero to infinity. Similar results are obtained if x-RVP is replaced with y-RVP.

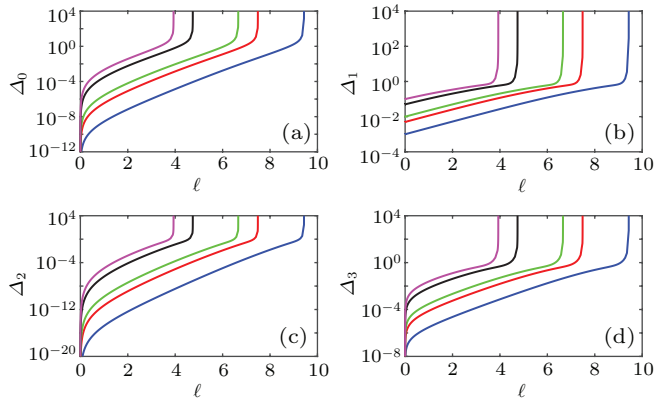


Fig. 6. Flows of disorder strength parameters at triple-TQCP with only x-RVP. Blue, red, green, black, magenta lines represent $\Delta_{1,0} = 0.001, 0.005, 0.01, 0.05, 0.1$, respectively.

Based on the above results, we conclude that RSP, x-RVP, and y-RVP affect the low-energy properties of triple-TQCP in a very similar way. In particular, any of them can generate all the rest types of disorders and drive the triple-TQCP to enter into a CDM phase.

Remarkably, we find that z-RVP plays a completely different role. To demonstrate this, we assume that Δ_3 takes a small bare value and set $\Delta_0 = \Delta_1 = \Delta_2 = 0$ at $\ell = 0$. As ℓ is growing, Δ_0, Δ_1, and Δ_2 do not flow at all, and remain zero for

all values of ℓ. From Fig. 7, we see that Δ_3 flows to the same constant value in the limit of $\ell \to \infty$, independent of the initial values of $\Delta_3(\ell = 0)$. This result indicates that z-RVP cannot generate the other types of disorders. Since Δ_3 does not diverge in the lowest energy limit, the triple-TQCP is stable and does not undergo any phase transition.

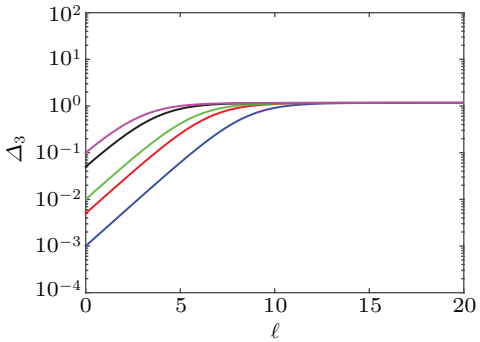


Fig. 7. Flows of disorder strength parameters at triple-TQCP with pure z-RVP. Blue, red, green, black, magenta lines represent $\Delta_{3,0} = 0.001, 0.005, 0.01, 0.05, 0.1$, respectively.

It is interesting to understand why z-RVP is so different from other disorders. We address this problem by analyzing the flow equation of the strength parameter Δ_3 for z-RVP. After setting $\Delta_0 = \Delta_1 = \Delta_2 = 0$, the flow equation (22) is simplified to

$$\frac{\mathrm{d}\Delta_3}{\mathrm{d}\ell} = \frac{5}{6}\Delta_3 - \frac{5}{7}\Delta_3^2. \tag{24}$$

To determine the fixed points of Δ_3, we need to solve the equation $\mathrm{d}\Delta_3/\mathrm{d}\ell = 0$. This equation has two solutions: $\Delta_3^* = 0$ and $\Delta_3^* = 7/6$. In the infrared region, the Gaussian fixed point $\Delta_3^* = 0$ is unstable, whereas the other fixed point $\Delta_3^* = 7/6$ is stable. Therefore, the triple-TQCP is stable in the clean limit ($\Delta_3 = 0$), but adding an arbitrary weak z-RVP to the system drives Δ_3 to flow to the constant value $\Delta_3^* = 7/6$. At the stable fixed point, the system should be identified as a disordered quantum critical state characterized by strong fermion-disorder interaction since Δ_3^* is large in magnitude.

The special role played by z-RVP should be attributed to the peculiar dispersion of the fermions excited at triple-TQCP. Recall the fermion dispersion at triple-TQCP has the following two terms:

$$\left(k_x^3 - 3k_x k_y^2\right)\sigma_1, \quad \left(k_y^3 - 3k_y k_x^2\right)\sigma_2. \tag{25}$$

These two terms are odd in fermion momentum. Owing to this property, the contribution of Fig. A1(c) and that of Fig. A1(d) are equal in magnitude but opposite in sign. Thus their contributions cancel each other, provided that z-RVP exists alone at triple-TQCP. For this reason, z-RVP cannot generate other disorders. The situation is distinct for double-TQCP, at which the fermion dispersion has the following two terms:

$$\left(k_x^2 - k_y^2\right)\sigma_1, \quad k_x k_y \sigma_2. \tag{26}$$

These two terms are even in fermion momentum. The contributions from Figs. A1(c) and A1(d) have the same sign, and thus do not cancel.

4. Summary and discussion

In summary, we have examined the stability of the TQCPs between topologically trivial BI phase and topologically nontrivial double- and triple-WSM phases against various disorders, including RSP and the three components of RVP. We carry out an extensive RG analysis and derive the coupled flow equations of all the model parameters. After comparing the impact of disorders, we show that these two TQCPs exhibit different behaviors when disorders are introduced. For double-TQCP, the system is unstable and can be readily turned into a CDM phase by any type of disorder. For triple-TQCP, the system is also unstable towards CDM phase due to RSP, x-RVP, or y-RVP. However, the triple-TQCP is stable against z-RVP.

The disordered quantum critical state realized by the stable fixed point of z-RVP at triple-TQCP deserves a more in-depth investigation. The strength parameter Δ_3^* exceeds unity, thus the system already falls into the strong-coupling regime. Two questions arise at this stage. Does this strong-coupling fixed point really exist at all? If the answer is positive, then is the value of Δ_3^* accurate? Our RG calculations are carried out by taking disorder strength parameters as the series expansion parameters. Once $\Delta_3^* > 1$, the reliability of the RG results needs to be examined more carefully. A possibility is that such a strong-coupling fixed point does exist, but the precise value of Δ_3^* should be computed with higher precision. It would be interesting to go beyond perturbative RG and use suitable non-perturbative techniques, such as exact diagonalization,[68,69] kernel polynomial method,[70–72] and Lanczos method,[71–73] to explore the putative strong-coupling fixed point driven by z-RVP at triple-TQCP and determine the precise value of Δ_3^*.

Apart from disorder scattering, the gapless fermions emergent at the double- and triple-TQCPs are also subjected to the Coulomb interaction. Recent works have revealed that the Coulomb interaction may lead to a series of interesting effects at double-TQCP[24,25] and at triple-TQCP[23] in the absence of disorders (i.e., clean limit). As a future project, we will study the influence of the interplay of disorder scattering and Coulomb interaction on the low-energy properties of double- and triple-TQCPs.

Appendix A: Derivation of RG equations

We fist derive the RG equations of model parameters for double-TQCP. The Feynman diagrams to be used in our calculations are collected in Fig. A1.

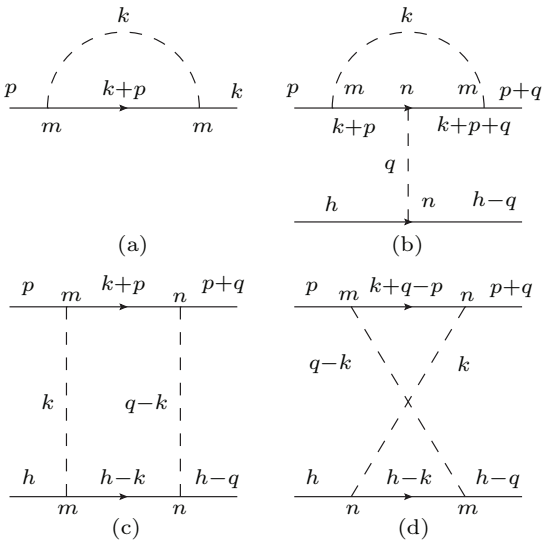


Fig. A1. The Feynman diagrams used in RG calculations. Diagram shown by (a) is the one-loop fermion self-energy correction. Diagrams shown by (b)–(d) are the one-loop corrections to the effective quartic coupling term given by Eq. (9).

The fermion self-energy function, represented by Fig. A1(a), is calculated at one-loop level as follows:

$$\Sigma_{\rm d}=\sum_{j=0}^{3}\Delta_j\int'\frac{{\rm d}^3\boldsymbol{k}}{(2\pi)^3}\sigma_j G_{\rm d0}(\omega,\boldsymbol{k})\sigma_j, \tag{A1}$$

where the prime appearing in $\int'$ implies that the integration is performed within the momentum shell defined at the beginning of Section 3. Substituting Eq. (3) into Eq. (A1), we obtain

$$\Sigma_{\rm d}=-{\rm i}\omega\Sigma_{{\rm d}\omega}, \tag{A2}$$

where

$$\Sigma_{{\rm d}\omega}=\sum_j\frac{\Gamma\left(\frac{1}{2}\right)\Gamma\left(\frac{1}{4}\right)\Delta_j}{16\pi^2\Gamma\left(\frac{3}{4}\right)A_\perp\sqrt{A_z\Lambda}}\ell. \tag{A3}$$

The correction to the the effective quartic term due to the diagram of Fig. A1(b) is

$$W_{\rm d}^{\rm (b)}=\sum_{i=0}W_{{\rm d}i}^{\rm (b)}, \tag{A4}$$

where

$$W_{{\rm d}i}^{\rm (b)}=\sum_j\Delta_i\Delta_j\left(\psi_a^\dagger\Gamma_i\psi_a\right)\times\int'\frac{{\rm d}^3\boldsymbol{k}}{(2\pi)^3}\left[\psi_b^\dagger\Gamma_j G_{\rm d0}(0,\boldsymbol{k})\Gamma_i G_{\rm d0}(0,\boldsymbol{k})\Gamma_j\psi_b\right]. \tag{A5}$$

Substituting the expression of fermion propagator as shown in Eq. (3) into Eq. (A5), we get

$$W_{\rm d0}^{\rm (b)}=\Delta_0\left(\Delta_0+\Delta_1+\Delta_2+\Delta_3\right)\times\frac{\Gamma\left(\frac{1}{2}\right)\Gamma\left(\frac{1}{4}\right)\ell}{12\pi^2\Gamma\left(\frac{3}{4}\right)A_\perp\sqrt{A_z\Lambda}}\left(\psi_a^\dagger\Gamma_0\psi_a\right)\left(\psi_b^\dagger\Gamma_0\psi_b\right), \tag{27}$$

$$W_{\rm d1}^{\rm (b)}=\Delta_0\left(-\Delta_0-\Delta_1+\Delta_2+\Delta_3\right)\times\frac{\Gamma\left(\frac{1}{2}\right)\Gamma\left(\frac{1}{4}\right)\ell}{36\pi^2\Gamma\left(\frac{3}{4}\right)A_\perp\sqrt{A_z\Lambda}}\left(\psi_a^\dagger\Gamma_1\psi_a\right)\left(\psi_b^\dagger\Gamma_1\psi_b\right), \tag{A7}$$

$$W_{\rm d2}^{\rm (b)}=\Delta_0\left(-\Delta_0+\Delta_1-\Delta_2+\Delta_3\right)\times\frac{\Gamma\left(\frac{1}{2}\right)\Gamma\left(\frac{1}{4}\right)\ell}{36\pi^2\Gamma\left(\frac{3}{4}\right)A_\perp\sqrt{A_z\Lambda}}\left(\psi_a^\dagger\Gamma_2\psi_a\right)\left(\psi_b^\dagger\Gamma_2\psi_b\right), \tag{A8}$$

$$W_{\rm d3}^{\rm (b)}=\Delta_0\left(-\Delta_0+\Delta_1+\Delta_2-\Delta_3\right)\times\frac{\Gamma\left(\frac{1}{2}\right)\Gamma\left(\frac{1}{4}\right)\ell}{36\pi^2\Gamma\left(\frac{3}{4}\right)A_\perp\sqrt{A_z\Lambda}}\left(\psi_a^\dagger\Gamma_3\psi_a\right)\left(\psi_b^\dagger\Gamma_3\psi_b\right). \tag{A9}$$

The corrections from Figs. A1(c) and A1(d) are

$$W_{\rm d}^{\rm (c)+(d)}=\sum_{i=0}^{3}\sum_{{\rm i}\le j\le 3}W_{{\rm d}ij}^{\rm (c)+(d)}, \tag{A10}$$

where

$$W_{{\rm d}ij}^{\rm (c)+(d)}=2\Delta_i\Delta_j\int'\frac{{\rm d}^3\boldsymbol{k}}{(2\pi)^3}\left(\psi_a^\dagger\Gamma_i G_{\rm d0}\Gamma_j\psi_a\right)\times\left\{\psi_b^\dagger\left[\Gamma_j G_{\rm d0}(0,\boldsymbol{k})\Gamma_i+\Gamma_i G_{\rm d0}(0,-\boldsymbol{k})\Gamma_j\right]\psi_b\right\}. \tag{A11}$$

Using the expression of the fermion propagator, we, after completing tedious calculations, arrive at

$$\begin{aligned}W_{\rm d}^{\rm (c)+(d)}=&\left\{2\Delta_0\left(\Delta_1+\Delta_2+\Delta_3\right)\left(\psi_a^\dagger\Gamma_0\psi_a\right)\left(\psi_b^\dagger\Gamma_0\psi_b\right)\right.\\&+\left[\Delta_0^2+\Delta_1^2+\Delta_2^2+\Delta_3^2+2\Delta_1\left(\Delta_2+\Delta_3\right)\right]\\&\times\left(\psi_a^\dagger\Gamma_1\psi_a\right)\left(\psi_b^\dagger\Gamma_1\psi_b\right)\\&+\left[\Delta_0^2+\Delta_1^2+\Delta_2^2+\Delta_3^2+2\Delta_2\left(\Delta_1+\Delta_3\right)\right]\\&\times\left(\psi_a^\dagger\Gamma_2\psi_a\right)\left(\psi_b^\dagger\Gamma_2\psi_b\right)\\&+\left[\Delta_0^2+\Delta_1^2+\Delta_2^2+\Delta_3^2+2\Delta_3(\Delta_1+\Delta_2)\right]\\&\times\left(\psi_a^\dagger\Gamma_3\psi_a\right)\left(\psi_b^\dagger\Gamma_3\psi_b\right)\left.\right\}\frac{\Gamma\left(\frac{1}{2}\right)\Gamma\left(\frac{1}{4}\right)\ell}{18\pi^2\Gamma\left(\frac{3}{4}\right)A_\perp\sqrt{A_z\Lambda}}.\end{aligned} \tag{A12}$$

According to Eqs. (27)–(A9) and (A12), the corrections for parameters Δ_i are

$$\delta\Delta_0=\left[3\Delta_0\left(\Delta_0+\Delta_1+\Delta_2+\Delta_3\right)+4\Delta_0\left(\Delta_1+\Delta_2+\Delta_3\right)\right]\times\frac{\Gamma\left(\frac{1}{2}\right)\Gamma\left(\frac{1}{4}\right)\ell}{18\pi^2\Gamma\left(\frac{3}{4}\right)A_\perp\sqrt{A_z\Lambda}}, \tag{A13}$$

$$\delta\Delta_1=\left[2\Delta_0^2+\Delta_1^2+2\Delta_2^2+2\Delta_3^2+\Delta_1\left(-\Delta_0+5\Delta_2+5\Delta_3\right)\right]\times\frac{\Gamma\left(\frac{1}{2}\right)\Gamma\left(\frac{1}{4}\right)\ell}{18\pi^2\Gamma\left(\frac{3}{4}\right)A_\perp\sqrt{A_z\Lambda}}, \tag{A14}$$

$$\delta\Delta_2=\left[2\Delta_0^2+2\Delta_1^2+\Delta_2^2+2\Delta_3^2+\Delta_2\left(-\Delta_0+5\Delta_1+5\Delta_3\right)\right]\times\frac{\Gamma\left(\frac{1}{2}\right)\Gamma\left(\frac{1}{4}\right)\ell}{18\pi^2\Gamma\left(\frac{3}{4}\right)A_\perp\sqrt{A_z\Lambda}}, \tag{A15}$$

$$\delta\Delta_3=\left[2\Delta_0^2+2\Delta_1^2+2\Delta_2^2+\Delta_3^2+\Delta_3\left(-\Delta_0+5\Delta_1+5\Delta_2\right)\right]\times\frac{\Gamma\left(\frac{1}{2}\right)\Gamma\left(\frac{1}{4}\right)\ell}{18\pi^2\Gamma\left(\frac{3}{4}\right)A_\perp\sqrt{A_z\Lambda}}. \tag{A16}$$

The original action has the form

$$S=\int\frac{{\rm d}\omega}{2\pi}\frac{{\rm d}^3\boldsymbol{k}}{(2\pi)^3}\psi^\dagger(\omega,\boldsymbol{k})[{\rm i}\omega-(A_\perp\left(k_x^2-k_y^2\right)\sigma_1$$

$$+2A_\perp k_x k_y\sigma_2+A_z k_z^2\sigma_3)]\psi(\omega,\boldsymbol{k})$$
$$+\sum_{j=0}^{3}\frac{\Delta_j}{2}\int\frac{\mathrm{d}\omega_1 d\omega_2\,\mathrm{d}^3\boldsymbol{k}_1\,\mathrm{d}^3\boldsymbol{k}_2\,\mathrm{d}^3\boldsymbol{k}_3}{(2\pi)^{11}}$$
$$\times[\psi_a(\omega_1,\boldsymbol{k}_1)\Gamma_j\psi_a(\omega_1,\boldsymbol{k}_1)]$$
$$\times[\psi_b(\omega_2,\boldsymbol{k}_3)\Gamma_j\psi_b(\omega_2,-\boldsymbol{k}_1-\boldsymbol{k}_2-\boldsymbol{k}_3)]. \tag{A17}$$

Incorporating the fermion self-energy Σ_{d} and corrections to the quartic fermion-fermion couplings, the action becomes

$$S=\int\frac{\mathrm{d}\omega}{2\pi}\frac{\mathrm{d}^3\boldsymbol{k}}{2\pi}\psi^\dagger(\omega,\boldsymbol{k})[\mathrm{i}\omega(1+\Sigma_{\mathrm{d}\omega})-(A_\perp(k_x^2-k_y^2)\sigma_1$$
$$+2A_\perp k_x k_y\sigma_2+A_z k_z^2\sigma_3)]\psi(\omega,\boldsymbol{k})$$
$$+\sum_{j=0}^{3}\frac{\Delta_j+\delta\Delta_j}{2}\int\frac{\mathrm{d}\omega_1 d\omega_2\,\mathrm{d}^3\boldsymbol{k}_1\,\mathrm{d}^3\boldsymbol{k}_2\,\mathrm{d}^3\boldsymbol{k}_3}{(2\pi)^{11}}$$
$$\times[\psi_a(\omega_1,\boldsymbol{k}_1)\Gamma_j\psi_a(\omega_1,\boldsymbol{k}_1)]$$
$$\times[\psi_b(\omega_2,\boldsymbol{k}_3)\Gamma_j\psi_b(\omega_2,-\boldsymbol{k}_1-\boldsymbol{k}_2-\boldsymbol{k}_3)]. \tag{A18}$$

In order to compare the interaction-corrected action to the original action, we make the following scaling transformations:

$$\omega=b\omega', \tag{A19}$$
$$k_x=b^{1/2}k_x', \tag{A20}$$
$$k_y=b^{1/2}k_y', \tag{A21}$$
$$k_z=b^{1/2}k_z', \tag{A22}$$
$$\psi=Z_\psi\psi', \tag{A23}$$
$$A_\perp'=Z_{A_\perp}A_\perp, \tag{A24}$$
$$A_z'=Z_{A_z}A_z, \tag{A25}$$
$$\Delta_0'=Z_0\Delta_0, \tag{A26}$$
$$\Delta_1'=Z_1\Delta_1, \tag{A27}$$
$$\Delta_2'=Z_2\Delta_2, \tag{A28}$$
$$\Delta_3'=Z_3\Delta_3. \tag{A29}$$

Then we obtain

$$Z_\psi=b^{7/4}(1+\Sigma_{\mathrm{d}\omega})^{1/2}, \tag{A30}$$
$$Z_{A_\perp}=(1-\Sigma_{\mathrm{d}\omega}), \tag{A31}$$
$$Z_{A_z}=(1-\Sigma_{\mathrm{d}\omega}), \tag{A32}$$
$$Z_0=(1-2\Sigma_{\mathrm{d}\omega})b^{-1/2}\left(1+\frac{\delta\Delta_0}{\Delta_0}\right), \tag{A33}$$
$$Z_1=(1-2\Sigma_{\mathrm{d}\omega})b^{-1/2}\left(1+\frac{\delta\Delta_1}{\Delta_1}\right), \tag{A34}$$
$$Z_2=(1-2\Sigma_{\mathrm{d}\omega})b^{-1/2}\left(1+\frac{\delta\Delta_2}{\Delta_2}\right), \tag{A35}$$
$$Z_3=(1-2\Sigma_{\mathrm{d}\omega})b^{-1/2}\left(1+\frac{\delta\Delta_3}{\Delta_3}\right). \tag{A36}$$

Based on all of these results, it is straightforward to derive the RG equations given by Eqs. (10)–(12) of the main text.

Then we derive the RG equations of the model parameters for triple-TQCP. The Feynman diagrams in need are also collected in Fig. A1.

The fermion self-energy function, represented by Fig. A1(a), at the one-loop level is calculated as

$$\Sigma_{\mathrm{t}}=\sum_{j=0}^{3}\Delta_j\int'\frac{\mathrm{d}^3\boldsymbol{k}}{(2\pi)^3}\sigma_j G_{\mathrm{t}0}(\omega,\boldsymbol{k})\sigma_j. \tag{A37}$$

Here, the integration is also carried out within the momentum shell defined in Section 3. Substituting Eq. (6) into Eq. (A36) leads to

$$\Sigma_{\mathrm{t}}=-\mathrm{i}\omega\Sigma_{\mathrm{t}\omega}, \tag{A38}$$

where

$$\Sigma_{\mathrm{t}\omega}=\sum_j\Delta_j\frac{\ell}{12\pi^2\Lambda^{5/6}}\frac{B(1/3,1/4)}{A^{1/2}B^{2/3}}. \tag{A39}$$

The correction to the effective quartic coupling term due to the diagram of Fig. A1(b) is

$$W_{\mathrm{t}}^{(\mathrm{b})}=\sum_{i=0}W_{\mathrm{t}i}^{(\mathrm{b})}, \tag{A40}$$

where

$$W_{\mathrm{t}i}^{(\mathrm{b})}=\sum_j\Delta_i\Delta_j\left(\psi_a^\dagger\Gamma_i\psi_a\right)$$
$$\times\int'\frac{\mathrm{d}^3\boldsymbol{k}}{(2\pi)^3}\left[\psi_b^\dagger\Gamma_j G_{\mathrm{t}0}(0,\boldsymbol{k})\Gamma_i G_{\mathrm{t}0}(0,\boldsymbol{k})\Gamma_j\psi_b\right]. \tag{A41}$$

Substituting the fermion propagator Eq. (6) into Eq. (A41), we get

$$W_{\mathrm{t}0}^{(\mathrm{b})}=\Delta_0(\Delta_0+\Delta_1+\Delta_2+\Delta_3)$$
$$\times\frac{\Gamma\left(\frac{1}{3}\right)\Gamma\left(\frac{1}{4}\right)\ell}{24\pi^2\Gamma\left(\frac{7}{12}\right)A^{1/2}B^{2/3}\Lambda^{5/6}}\left(\psi_a^\dagger\Gamma_0\psi_a\right)\left(\psi_b^\dagger\Gamma_0\psi_b\right), \tag{A42}$$

$$W_{\mathrm{t}1}^{(\mathrm{b})}=\Delta_0(-\Delta_0-\Delta_1+\Delta_2+\Delta_3)$$
$$\times\frac{\Gamma\left(\frac{1}{3}\right)\Gamma\left(\frac{1}{4}\right)\ell}{56\pi^2\Gamma\left(\frac{7}{12}\right)A^{1/2}B^{2/3}\Lambda^{5/6}}\left(\psi_a^\dagger\Gamma_1\psi_a\right)\left(\psi_b^\dagger\Gamma_1\psi_b\right), \tag{A43}$$

$$W_{\mathrm{t}2}^{(\mathrm{b})}=\Delta_0(-\Delta_0+\Delta_1-\Delta_2+\Delta_3)$$
$$\times\frac{\Gamma\left(\frac{1}{3}\right)\Gamma\left(\frac{1}{4}\right)\ell}{56\pi^2\Gamma\left(\frac{7}{12}\right)A^{1/2}B^{2/3}\Lambda^{5/6}}\left(\psi_a^\dagger\Gamma_2\psi_a\right)\left(\psi_b^\dagger\Gamma_2\psi_b\right), \tag{A44}$$

$$W_{\mathrm{t}3}^{(\mathrm{b})}=\Delta_0(-\Delta_0+\Delta_1+\Delta_2-\Delta_3)$$
$$\times\frac{\Gamma\left(\frac{1}{3}\right)\Gamma\left(\frac{1}{4}\right)\ell}{168\pi^2\Gamma\left(\frac{7}{12}\right)A^{1/2}B^{2/3}\Lambda^{5/6}}\left(\psi_a^\dagger\Gamma_3\psi_a\right)\left(\psi_b^\dagger\Gamma_3\psi_b\right). \tag{A45}$$

The corrections from Figs. A1(c) and A1(d) are

$$W_{\mathrm{t}}^{(\mathrm{c})+(\mathrm{d})}=\sum_{i=0}^{3}\sum_{\mathrm{i}\le j\le 3}W_{\mathrm{t}ij}^{(\mathrm{c})+(\mathrm{d})}, \tag{A46}$$

where

$$W_{\mathrm{t}ij}^{(\mathrm{c})+(\mathrm{d})} = 2\Delta_i\Delta_j \int' \frac{\mathrm{d}^3\boldsymbol{k}}{(2\pi)^3} \left(\psi_a^\dagger \Gamma_i G_{\mathrm{t}0} \Gamma_j \psi_a\right) \times \left\{\psi_b^\dagger \left[\Gamma_j G_{\mathrm{t}0}(0,\boldsymbol{k})\Gamma_i + \Gamma_i G_{\mathrm{t}0}(0,-\boldsymbol{k})\Gamma_j\right]\psi_b\right\}. \tag{A47}$$

Straightforward computations of this integral give rise to

$$\begin{aligned} W_{\mathrm{t}}^{(\mathrm{c})+(\mathrm{d})} = &\left\{4\left(\frac{1}{84}\Delta_2\Delta_3 + \frac{1}{84}\Delta_1\Delta_3 + \frac{1}{56}\Delta_0\Delta_3\right)\right. \\ &\times \left(\psi_a^\dagger\Gamma_0\psi_a\right)\left(\psi_b^\dagger\Gamma_0\psi_b\right) \\ &+4\left(\frac{1}{84}\Delta_0\Delta_3 + \frac{1}{56}\Delta_1\Delta_3\right)\left(\psi_a^\dagger\Gamma_1\psi_a\right)\left(\psi_b^\dagger\Gamma_1\psi_b\right) \\ &+4\left(\frac{1}{84}\Delta_0\Delta_3 + \frac{1}{56}\Delta_2\Delta_3\right)\left(\psi_a^\dagger\Gamma_2\psi_a\right)\left(\psi_b^\dagger\Gamma_2\psi_b\right) \\ &+\left[4\left(\frac{1}{84}\Delta_0\Delta_2 + \frac{1}{84}\Delta_0\Delta_1\right) + 2\right. \\ &\left.\left.\times\frac{1}{56}\left(\Delta_0^2+\Delta_1^2+\Delta_2^2+\Delta_3^2\right)\right]\left(\psi_a^\dagger\Gamma_3\psi_a\right)\left(\psi_b^\dagger\Gamma_3\psi_b\right)\right\} \\ &\times \frac{\Gamma\left(\frac{1}{3}\right)\Gamma\left(\frac{1}{4}\right)\ell}{\pi^2\Gamma\left(\frac{7}{12}\right)A^{1/2}B^{2/3}\Lambda^{5/6}}. \end{aligned} \tag{A48}$$

According to Eqs. (A42)–(A45) and (A48), the corrections for Δ_i satisfy

$$\begin{aligned} \delta\Delta_0 = &\left(7\Delta_0(\Delta_0+\Delta_1+\Delta_2+\Delta_3)\right. \\ &\left.+16\Delta_2\Delta_3+16\Delta_1\Delta_3+24\Delta_0\Delta_3\right) \\ &\times\frac{\Gamma\left(\frac{1}{3}\right)\Gamma\left(\frac{1}{4}\right)\ell}{168\pi^2\Gamma\left(\frac{7}{12}\right)A^{1/2}B^{2/3}\Lambda^{5/6}}, \end{aligned} \tag{A49}$$

$$\begin{aligned} \delta\Delta_1 = &\left(3\Delta_0(-\Delta_0-\Delta_1+\Delta_2+\Delta_3)+16\Delta_0\Delta_3+24\Delta_1\Delta_3\right) \\ &\times\frac{\Gamma\left(\frac{1}{3}\right)\Gamma\left(\frac{1}{4}\right)\ell}{168\pi^2\Gamma\left(\frac{7}{12}\right)A^{1/2}B^{2/3}\Lambda^{5/6}}, \end{aligned} \tag{A50}$$

$$\begin{aligned} \delta\Delta_2 = &\left(3\Delta_0(-\Delta_0+\Delta_1-\Delta_2+\Delta_3)+16\Delta_0\Delta_3+24\Delta_2\Delta_3\right) \\ &\times\frac{\Gamma\left(\frac{1}{3}\right)\Gamma\left(\frac{1}{4}\right)\ell}{168\pi^2\Gamma\left(\frac{7}{12}\right)A^{1/2}B^{2/3}\Lambda^{5/6}}, \end{aligned} \tag{A51}$$

$$\begin{aligned} \delta\Delta_3 = &\left[\Delta_0(-\Delta_0+\Delta_1+\Delta_2-\Delta_3)+16\left(\Delta_0\Delta_2+\Delta_0\Delta_1\right)\right. \\ &\left.+12\left(\Delta_0^2+\Delta_1^2+\Delta_2^2+\Delta_3^2\right)\right] \\ &\times\frac{\Gamma\left(\frac{1}{3}\right)\Gamma\left(\frac{1}{4}\right)\ell}{168\pi^2\Gamma\left(\frac{7}{12}\right)A^{1/2}B^{2/3}\Lambda^{5/6}}. \end{aligned} \tag{A52}$$

The original action is of the form

$$\begin{aligned} S = &\int\frac{\mathrm{d}\omega}{2\pi}\frac{\mathrm{d}^3\boldsymbol{k}}{(2\pi)^3}\psi^\dagger(\omega,\boldsymbol{k})\left(\mathrm{i}\omega - B[(k_x^3-3k_xk_y^2)\sigma_x\right. \\ &\left.+(k_y^3-3k_yk_x^2)\sigma_y] - Ak_z^2\sigma_z\right)\psi(\omega,\boldsymbol{k}) \\ &+\sum_{j=0}^{3}\frac{\Delta_j}{2}\int\frac{\mathrm{d}\omega_1\,\mathrm{d}\omega_2\,\mathrm{d}^3\boldsymbol{k}_1\,\mathrm{d}^3\boldsymbol{k}_2\,\mathrm{d}^3\boldsymbol{k}_3}{(2\pi)^{11}} \\ &\times\left[\psi_a(\omega_1,\boldsymbol{k}_1)\Gamma_j\psi_a(\omega_1,\boldsymbol{k}_1)\right] \\ &\times\left[\psi_b(\omega_2,\boldsymbol{k}_3)\Gamma_j\psi_b(\omega_2,-\boldsymbol{k}_1-\boldsymbol{k}_2-\boldsymbol{k}_3)\right]. \end{aligned} \tag{A53}$$

Incorporating the fermion self-energy Σ_{t} and the corrections to the quartic coupling changes the action to

$$\begin{aligned} S = &\int\frac{\mathrm{d}\omega}{2\pi}\frac{\mathrm{d}^3\boldsymbol{k}}{(2\pi)^3}\psi^\dagger(\omega,\boldsymbol{k})\left(\mathrm{i}\omega(1+\Sigma_{\mathrm{t}\omega}) - B[(k_x^3-3k_xk_y^2)\sigma_x\right. \\ &\left.+(k_y^3-3k_yk_x^2)\sigma_y] - Ak_z^2\sigma_z\right)\psi(\omega,\boldsymbol{k}) \\ &+\sum_{j=0}^{3}\frac{\Delta_j+\delta\Delta_j}{2}\int\frac{\mathrm{d}\omega_1 d\omega_2\,\mathrm{d}^3\boldsymbol{k}_1\,\mathrm{d}^3\boldsymbol{k}_2\,\mathrm{d}^3\boldsymbol{k}_3}{(2\pi)^{11}} \\ &\times\left(\psi_a(\omega_1,\boldsymbol{k}_1)\Gamma_j\psi_a(\omega_1,\boldsymbol{k}_1)\right)\left(\psi_b(\omega_2,\boldsymbol{k}_3)\right. \\ &\left.\times\Gamma_j\psi_b(\omega_2,-\boldsymbol{k}_1-\boldsymbol{k}_2-\boldsymbol{k}_3)\right). \end{aligned} \tag{A54}$$

Then make the following re-scaling transformations:

$$\omega = b\omega', \tag{A55}$$
$$k_x = b^{1/3}k_x', \tag{A56}$$
$$k_y = b^{1/3}k_y', \tag{A57}$$
$$k_z = b^{1/2}k_z', \tag{A58}$$
$$\psi = Z_\psi\psi', \tag{A59}$$
$$B' = Z_B B, \tag{A60}$$
$$A' = Z_A A, \tag{A61}$$
$$\Delta_0' = Z_0\Delta_0, \tag{A62}$$
$$\Delta_1' = Z_1\Delta_1, \tag{A63}$$
$$\Delta_2' = Z_2\Delta_2, \tag{A64}$$
$$\Delta_3' = Z_3\Delta_3. \tag{A65}$$

The model parameters are renormalized by the fermion-disorder interaction as follows:

$$Z_\psi = b^{19/12}\left(1+\Sigma_{\mathrm{t}\omega}\right)^{1/2}, \tag{A66}$$
$$Z_B = \left(1-\Sigma_{\mathrm{t}\omega}\right), \tag{A67}$$
$$Z_A = \left(1-\Sigma_{\mathrm{t}\omega}\right), \tag{A68}$$
$$Z_0 = \left(1-2\Sigma_{\mathrm{t}\omega}\right)b^{-5/6}\left(1+\frac{\delta\Delta_0}{\Delta_0}\right), \tag{A69}$$
$$Z_1 = \left(1-2\Sigma_{\mathrm{t}\omega}\right)b^{-5/6}\left(1+\frac{\delta\Delta_1}{\Delta_1}\right), \tag{A70}$$
$$Z_2 = \left(1-2\Sigma_{\mathrm{t}\omega}\right)b^{-5/6}\left(1+\frac{\delta\Delta_2}{\Delta_2}\right), \tag{A71}$$
$$Z_3 = \left(1-2\Sigma_{\mathrm{t}\omega}\right)b^{-5/6}\left(1+\frac{\delta\Delta_3}{\Delta_3}\right). \tag{A72}$$

From the transformations Eqs. (A60)–(A65), the relations Eq. (A67)–(A72), the expressions (A39) and (A49)–(A49), we eventually obtain the RG equations shown in Eqs. (17)–(22) in the main text.

Acknowledgements

Project supported by the Natural Science Foundation of Anhui Province, China (Grant No. 2208085MA11) and the National Natural Science Foundation of China (Grants Nos. 11974356, 12274414, and U1832209).

References

[1] Vafek O and Vishwanath A 2014 *Annu. Rev. Condens. Matter Phys.* **5** 83
[2] Wehling T O, Black-Schaffer A M and Balatsky A V 2014 *Adv. Phys.* **63** 1
[3] Yang B J and Nagaosa N 2014 *Nat. Commun.* **5** 4898
[4] Weng H, Dai X and Fang Z 2016 *J. Phys.-Condens. Matter* **28** 303001
[5] Fang C, Weng H, Dai X and Fang Z 2016 *Chin. Phys. B* **25** 117106
[6] Armitage N P, Mele E J and Vishwanath A 2018 *Rev. Mod. Phys.* **90** 015001
[7] Lv B Q, Qian T and Ding H 2021 *Rev. Mod. Phys.* **93** 025002
[8] Hasan M Z, Chang G, Belopolski I, Bian G, Xu S Y and Yin J X 2021 *Nat Rev Mater* **6** 784
[9] Lu H Z and Shen S Q 2016 *Chin. Phys. B* **25** 117202
[10] Wang H and Wang J 2018 *Chin. Phys. B* **27** 107402
[11] Feng X L, Zhu J J, Wu W K and Yang S Y 2021 *Chin. Phys. B* **30** 107304
[12] Son D T and Spivak B Z 2013 *Phys. Rev. B* **88** 104412
[13] Burkov A A 2017 *Phys. Rev. B* **96** 041110
[14] Nandy S, Sharma G, Taraphder A and Tewari S 2017 *Phys. Rev. Lett.* **119** 176804
[15] Goswami P and Chakravarty S 2011 *Phys. Rev. Lett.* **107** 196803
[16] Dietl P, Piéchon F and Montambaux G 2008 *Phys. Rev. Lett.* **100** 236405
[17] Montambaux G, Piéchon F, Fuchs J N and Goerbig M O 2009 *Phys. Rev. B* **80** 153412
[18] Isobe H, Yang B J, Chubukov A, Schmalian J and Nagaosa N 2016 *Phys. Rev. Lett.* **116** 076803
[19] Cho G Y and Moon E G 2016 *Sci. Rep.* **6** 19198
[20] Wang J R, Liu G Z and Zhang C J 2017 *Phys. Rev. B* **95** 075129
[21] Yang B J, Bahramy M S, Arita R, Isobe H, Moon E G and Nagaosa N 2013 *Phys. Rev. Lett.* **110** 086402
[22] Yang B J and Nagaosa N 2014 *Nat. Commun.* **5** 4898
[23] Wang J R, Liu G Z and Zhang C J 2019 *Phys. Rev. B* **99** 195119
[24] Han S E, Lee C, Moon E G and Min H 2019 *Phys. Rev. Lett.* **122** 187601
[25] Zhang S X, Jian S K and Yao H 2021 *Phys. Rev. B* **103** 165129
[26] Xu S Y, Xia Y, Wray L A, Jia S, Meier F, Dil J H, Osterwalder J, Slomski B, Bansil A, Lin H, Cava R J and Hasan M Z 2011 *Science* **332** 560
[27] Sato T, Segawa K, Kosaka K, Souma S, Nakayama K, Eto K, Minami T, Ando Y and Takahashi T 2011 *Nat. Phys.* **7** 840
[28] Wu L, Brahlek M, Aguilar R V, Stier A V, Morris C M, Lubashevsky Y, Bilbro L S, Bansal N, Oh S and Armitage N P 2013 *Nat. Phys.* **9** 410
[29] Brahlek M, Bansal N, Koirala N, Xu S Y, Neupane M, Liu C, Hasan M Z and Oh S 2012 *Phys. Rev. Lett.* **109** 186403
[30] Xu G, Weng H, Wang Z, Dai X and Fang Z 2011 *Phys. Rev. Lett.* **107** 186806
[31] Fang C, Gilbert M J, Dai X and Bernevig B A 2012 *Phys. Rev. Lett.* **108** 266802
[32] Lai H H 2015 *Phys. Rev. B* **91** 235131
[33] Jian S K and Yao H 2015 *Phys. Rev. B* **92** 045121
[34] Bera S, Sau J D and Roy B 2016 *Phys. Rev. B* **93** 201302
[35] Sbierski B, Trescher M, Bergholtz E J and Brouwer P W 2017 *Phys. Rev. B* **95** 115104
[36] Roy B, Goswami P and Juričić V 2017 *Phys. Rev. B* **95** 201102
[37] Wang J R, Liu G Z and Zhang C J 2017 *Phys. Rev. B* **96** 165142
[38] Zhang S X, Jian S K and Yao H 2017 *Phys. Rev. B* **96** 241111
[39] Wang J R, Liu G Z and Zhang C J 2018 *Phys. Rev. B* **98** 205113
[40] Huang S M, Xu S Y, Belopolski I, Lee C C, Chang G, Chang T R, Wang B K, Alidoust N, Bian G, Neupane M, Sanchez D, Zheng H, Jeng H T, Bansil A, Neupert T, Lin H and Hasan M Z 2016 *Proc. Natl. Acad. Sci. USA* **113** 1180
[41] Liu Q and Zunger A 2017 *Phys. Rev. X* **7** 021019
[42] Chen W J, Xiao M and Chan C T 2016 *Nat. Commun.* **7** 13038
[43] Chang M L, Xiao M, Chen W J and Chan C T 2017 *Phys. Rev. B* **95** 125136
[44] Ludwig A W W, Fisher M P A, Shankar R and Grinstein G 1994 *Phys. Rev. B* **50** 7526
[45] Nersesyan A A, Tsvelik A M and Wenger F 1994 *Phys. Rev. Lett.* **72** 2628
[46] Ostrovsky P M, Gornyi I V and Mirlin A D 2006 *Phys. Rev. B* **74** 235443
[47] Evers F and Mirlin A D 2008 *Rev. Mod. Phys.* **80** 1355
[48] Fradkin E 1986 *Phys. Rev. B* **33** 3263
[49] Shindou R and Murakami S 2009 *Phys. Rev. B* **79** 045321
[50] Ominato Y and Koshino M 2014 *Phys. Rev. B* **89** 054202
[51] Sbierski B, Pohl G, Bergholtz E J and Brouwer P W 2014 *Phys. Rev. Lett.* **113** 026602
[52] Roy B and Das Sarma S 2014 *Phys. Rev. B* **90** 241112
[53] Syzranov S V, Ostrovsky P M, Gurarie V and Radzihovsky L 2016 *Phys. Rev. B* **93** 155113
[54] Syzranov S V and Radzihovsky L 2018 *Annu. Rev. Condens. Matter Phys.* **9** 35
[55] Carpentier D, Fedorenko A A and Orignac E 2013 *Euro. Phys. Lett.* **102** 67010
[56] Sbierski B, Decker K S C and Brouwer P W 2016 *Phys. Rev. B* **94** 220202
[57] Zhao P L, Wang J R, Wang A M and Liu G Z 2016 *Phys. Rev. B* **94** 195114
[58] Nandkishore R M and Parameswaran S A 2017 *Phys. Rev. B* **95** 205106
[59] Sikkenk T S and Fritz L 2017 *Phys. Rev. B* **96** 155121
[60] Yang Z K, Wang J R and Liu G Z 2018 *Phys. Rev. B* **98** 195123
[61] Luo X, Xu B, Ohtsuki T and Shindou R 2018 *Phys. Rev. B* **98** 045129
[62] Luo X, Ohtsuki T and Shindou R 2018 *Phys. Rev. B* **98** 020201
[63] Roy B, Slager R J and Juričić V 2018 *Phys. Rev. X* **8** 031076
[64] Ning Z, Fu B, Shi Q and Wang X 2020 *Chin. Phys. B* **29** 077202
[65] Wang J, Liu G Z and Kleinert H 2011 *Phys. Rev. B* **83** 214503
[66] Stauber T, Guinea F and Vozmediano M A H 2005 *Phys. Rev. B* **71** 041406
[67] Shankar R 1994 *Rev. Mod. Phys.* **66** 129
[68] Park M J, Basa B and Gilbert M J 2017 *Phys. Rev. B* **95** 094201
[69] Zhu W and Sheng D N 2019 *Phys. Rev. Lett.* **123** 056804
[70] Pixley J H, Goswami P and Das Sarma S 2015 *Phys. Rev. Lett.* **115** 076601
[71] Pixley J H, Wilson J H, Huse D A and Gopalakrishnan S 2018 *Phys. Rev. Lett.* **120** 207604
[72] Gonçalves M, Ribeiro P, Castro E V and Araújo M A N 2020 *Phys. Rev. Lett.* **124** 136405
[73] Fu B, Zhu W, Shi Q, Li Q, Yang J and Zhang Z 2017 *Phys. Rev. Lett.* **118** 146401